PERGAMON

Vision Research 39 (1999) 947–959

Vision Research

Contour integration in the peripheral field

Robert F. Hess *, Steven C. Dakin

McGill Vision Research Unit, Department of Ophthalmology, McGill University, 687 Pine Avenue West, Room H4-14, Montreal, Quebec, Canada

Received 22 May 1997; received in revised form 9 October 1997; accepted 6 April 1998

Abstract

Contour integration was measured in the normal peripheral field to determine if an explanation based solely on the known peripheral positional uncertainty was sufficient to explain performance. The task involved the detection of paths composed of micropatterns with correlated carrier orientations embedded in a field of similar micropatterns of random position and orientation (Field, D. J., Hayes A., & Hess, R. F. (1993). Vision Research, 33, 173–193). The intrinsic positional uncertainty for each eccentric locus was measured with the same stimulus and it did not account for levels of peripheral performance. We show that peripheral performance on this task does not get worse with eccentricity beyond about 10° and that these results can be modeled by simple filtering without any subsequent cellular linking interactions. © 1998 Elsevier Science Ltd. All rights reserved.

Keywords: Association; Contour integration; Periphery; Positional uncertainty

1. Introduction

There are important differences in the processing capabilities of central and peripheral vision. For spatial vision, the periphery exhibits reduced acuity (Wertheim, 1994), contact sensitivity (Robson & Graham, 1981; Pointer & Hess, 1989) and positional accuracy (Westheimer, 1982). The available evidence suggests that the site of these limitations is postreceptoral (Anderson, Mullen & Hess, 1991; Hess & Hayes, 1994) through at an early stage of visual processing. Here we ask whether a higher visual process, contour integration, is selectively reduced in peripheral vision. This visual process requires cooperative interactions between cortical cells of different orientation preference and has the great advantage of providing information on how the outputs of cortical cells are combined (Field, Hayes & Hess, 1993). In this respect it is particularly relevant to ask whether these rules of association are similar in foveal and peripheral vision.

To answer this question we have been careful to control, for the known acuity, contrast sensitivity and positional uncertainty difference in peripheral function. To control for the decreased peripheral acuity we use spatial frequency narrowband stimuli which are within the spatial sampling limits of the peripheral loci that we investigate (Wang, Thibos & Bradley, 1996). To control for the known contrast sensitivity loss in the periphery we use stimuli that are very suprathreshold in a task which has already been shown to saturate at quite low contrasts (McIlhagga & Mullen, 1996). To control for the known positional uncertainty of the periphery we measure the incremental positional uncertainty for our stimuli and use this to estimate the resident internal pedestal of uncertainty associated with each eccentric locus that we test. In so doing we estimate to what extent this underlying internal peripheral uncertainty can account for any reduction in performance on our contour integration task.

Our results suggest that peripheral performance is not limited by positional uncertainty and furthermore that performance does not deteriorate significantly beyond 10°. This level of performance can be explained by a simple filtering model without the need to invoke interactions between cells tuned to different orientations.

* Corresponding author. Fax: +1 514 8431691; e-mail: rhess@bradman.vision.mcgill.ca.

0042-6989/98/$ - see front matter
PII: S0042-6989(98)00152-7

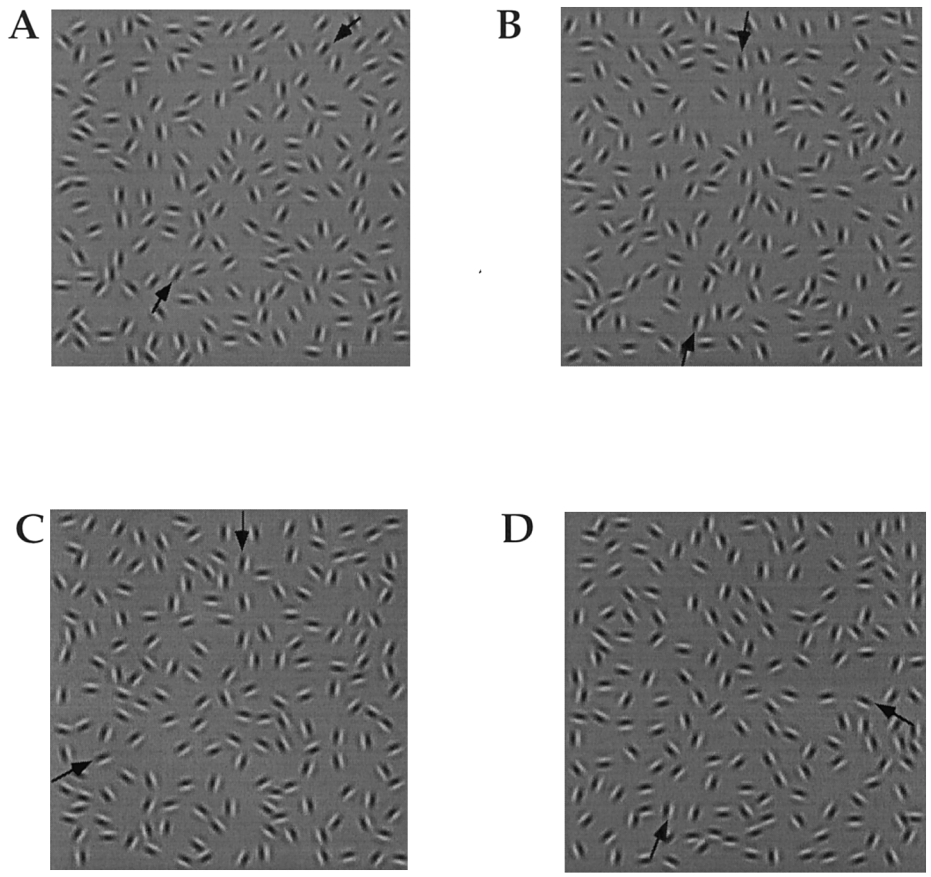

Fig. 1. A path comprising eight micropatterns (end points indicted by arrows) is imbedded in a field of randomly oriented micropatterns of the same form. Paths are shown for different path angles (Fig. 2): A, 0°; B, 10°; C, 20°; and D, 30°.

2. Methods

In all experiments the observers' task was to identify which of two presentations contained the 'path stimulus'. A path stimulus consisted of a set of oriented Gabor elements aligned along a common contour, embedded in a background of similar, but randomly oriented, Gabor elements. A no-path stimulus consisted of just randomly placed and randomly oriented Gabor elements. Gabor elements were used to control the spatial frequency composition of the stimuli so that the path could not be extracted by a single broad band detector. By using such stimuli we hope to gain a better understanding of the combinatorial rules which govern the outputs of visual neurones used in the extraction of the path from the background elements.

2.1. Stimuli

Oriented spatial frequency bandpass elements were used in this study; the oriented Gabor elements were defined by Eq. (1)

$$g(x, y, \theta) = c*\sin(2\pi f*(x \sin\theta + y \cos\theta)) \times \exp\left(-\frac{x^2+y^2}{2\sigma^2}\right) \quad (1)$$

where is the element orientation, from 0 to 360°, (x, y) is the distance in degrees from the element center, and c is the contrast. The sinusoidal frequency, f was 0.05 c/pixel, the space constant, was $0.4 \times \lambda$. The contrast was 90% and the spatial frequency was 3 c/d.

A no-path stimulus was constructed in the following way. A 624 pixel wide square was divided into a 13×13 grid of equally sized cells. A Gabor element of random orientation was placed randomly in each display cell, with the restriction that each cell contain the center of only one Gabor element. This eliminates the clumping of elements due to random placement. The elements were also placed to avoid overlap as much as possible. An empty cell occurred if the cells' Gabor patch could not be placed without significantly overlapping any of its neighbors (i.e. crowded out by its neighbors). There were fewer than four per image.

A path stimulus consisted of two parts; the path itself and the background (Fig. 1). The construction of the

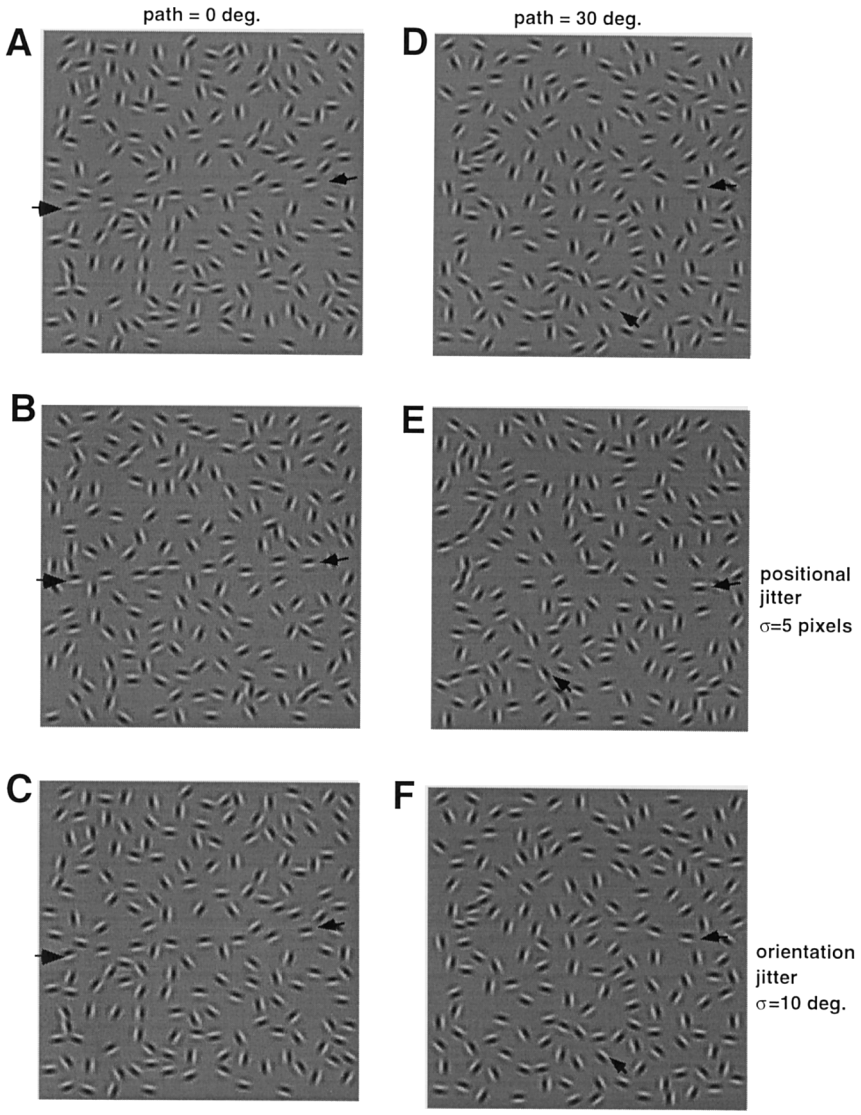

Fig. 2. Examples of 0 and 30° paths with Gaussian distributed jitter added to either the path element angle or the path element position.

path is described in detail elsewhere (Field, Hayes & Hess, 1993). The path had a backbone of eight invisible line segments; each line segment was of length 67 pixels and the line segments joined at an angle uniformly distributed from -4 to $+4°$. is called the path angle. Gabor elements were then placed at the middle of each line segment. The orientation of each element was the same as the orientation of the line segment on which it was placed. The element angle which is defined as the angle that the oriented element makes with the invisible backbone would be zero in this case. In some experiments (see Fig. 2 for demonstration and Fig. 4 for data), the element angle was determined by a random variable. Finally to avoid random changes in path detection due to random path closure (which can have significant effects on path detection; Kovacs & Julesz, 1993), the path was checked to ensure that it neither intersected itself, nor looped back on itself. If so it was discarded and a new path generated.

The entire path contour was inserted into the display at a random location, ensuring the centers of the Gabor elements occupied different cells. Finally, empty cells were filled with randomly oriented Gabor elements, as described in the no path stimulus above. The average length of each backbone line segment (67 pixels) was the same as the average distance between neighboring Gabor elements in the background. Previous studies (Field, Hayes & Hess, 1993; McIlhagga & Mullen, 1996) have shown that path detection varies inversely with the length of the backbone line segments in a smooth manner, so the choice of segment length was not critical.

Neither the local nor the global element density served as a cue to detection of path from no-path stimuli. The average distance from an element to its

neighbor was no different for path and no-path stimuli. Secondly, the total number of empty cells was the same for path and no-path stimuli. If element density is not a cue then path detectability should be solely due to the alignment of elements in the path, since nothing else distinguishes path from no-path stimuli. Hess & Field (1995) and McIlhagga & Mullen (1996) confirmed this in control experiments where orientation of the path elements was randomized; they found that the path could not be detected, even under extended viewing conditions, regardless of the path angle .

2.2. Apparatus and experimental procedures

All stimuli were displayed on a Sony Trinitron monitor driven by a Sun Sparc station 2 computer, which generated stimuli on-line and controlled the display and data collection. The mean luminance was 35 cd/m^2. The screen size was $12 \times 15°$ and the viewing distance (1.15 m) did not vary with eccentricity. The monitor was driven by an 8 bit D/A converter and an 8 bit frame buffer. The monitor was gamma corrected in software, and behaved linearly when displaying high spatial frequencies (12 cpd square wave) up to 90% contrast. It was viewed in a lit room. Each experimental run consisted of a block of 50 trials in each of which two images were presented (a path in a noise background and a noise background image alone), for 2.0 s, in random order. The subjects' task was to indicate with a button press which image contained the path. In each run, the path angle was set to 0, 5, 10, 20, 30, 40° etc. Typically, each block was repeated twice to obtain at least 100 trials per path angle. The parameter values are given in screen units (Table 1 in Appendix A) because the stimulus was kept constant on the screen for all eccentric measurements.

2.3. Control experiments

In a number of control experiments we varied different parameters of our stimuli to evaluate their effect on peripheral performance. This included the exposure duration which had an abrupt onset and offset, the number of path elements, the element contrast, the accuracy with which path elements were positioned on their invisible backbones and the accuracy with which the element orientation was aligned along its invisible backbone. In the latter two cases, the random variable had a Gaussian distribution with variable σ (Fig. 2).

Table 1
Chi-Square values for the fit of the filter model to data from two subjects at the eccentricities tested

Eccentricity (°)	RFH	SCD
10	2.7 (d.f. = 7; $P<$ 0.05)	3.3 (d.f. = 7; $P<0.05$)
20	4.1 (d.f. = 4; $P<$ 0.05)	0.64 (d.f. = 3; $P<0.05$)
25°		1.1 (d.f. = 4; $P<0.05$)
30	3.6 (d.f. = 3; $P<$ 0.05)	0.78 (d.f. = 6; $P<0.05$)

2.4. Positional uncertainty

We measured the positional uncertainty of the periphery using a 2AFC discrimination task between a path composed of accurately positioned elements (a pedestal of zero uncertainty) and an identical path composed of elements aligned along the path with a variable amount of positional uncertainty (2-D Gaussian distributed). For these measurements there were no background elements (just the path elements in isolation on a mean luminance background). A staircase procedure (200 trials) was used to collect psychometric data in the critical range and parameters estimated by fitting a Weibull function to the psychometric data. This function had the form Eq. (2)

$$p(x) = 1 - 0.5 * \exp\left(-\left[\frac{x}{c}\right]^b \right) \quad (2)$$

where $p(x)$ is the probability of correctly discriminating between the two paths at a jitter variance of x. c represents the threshold and b the slope of the psychometric function. Unequal trials were handled by the fitting procedure which used maximum likelihood.

The logic of this approach is as follows. From a measurement of the incremental positional sensitivity (measured on a zero pedestal of stimulus uncertainty), at various path angles and eccentric loci, we need to work back to what internal (termed intrinsic) pedestal of uncertainty produced this performance. To determine the level of intrinsic uncertainty we reversed the above procedure using the fovea. This time the increment was fixed at the level previously determined for the periphery and the pedestal uncertainty was adjusted in the manner described above. The threshold (derived in a manner identical to that described above) represented the internal uncertainty at a particular peripheral locus which corresponded to the previously determined incremental sensitivity at that peripheral locus. This assumes that the function describing positional uncertainty/pedestal uncertainty for the periphery is merely a laterally shifted version of that for the fovea. In other words, the external variance and the internal variance (i.e. uncertainty) are additive (for support see Hess & Watt, 1990). We undertook this determination for at least three different path angles at each eccentric locus.

This approach is best illustrated by example. Assume the periphery introduces an intrinsic jitter in the encoded position of each path element which is large

compared with that of the fovea (we assume that the foveal uncertainty is negligible). That is, the difference between the true position of the element and its encoded position is a Gaussian random variable with a variance of A. If we now ask the periphery to discriminate between an unjittered and a jittered path (of variance S) then, internally, the periphery must discriminate between jitters of A and $A+S$, since intrinsic jitter A is added to both stimuli. Suppose the periphery attains 75% correct at a stimulus jitter of S_A. We can simulate the peripheral condition in the fovea by doing jitter discrimination between a pedestal jitter P and a test jitter $P+S$. Suppose that the fovea attains 75% correct at S_G. Now find the specific pedestal jitter P^* that makes $S_G = S_A$. When this happens we must have $P^* = A$, so P^* is the intrinsic jitter in the periphery.

It's is worth emphasizing that this argument is not circular, i.e. the pedestal jitter measured in the isolated path case won't inevitably produce the same performance when the path is embedded in the background. The latter case involves detection of the path in noise, the former discrimination of path regularity without noise.

The carrier spatial frequency of the Gabor micropatterns was set to be within the spatial sampling range of the eccentric loci tested (Wang, Thibos & Bradley, 1996). We verified that this was the case by ensuring that at each eccentric loci subjects could correctly perform a 2AFC horizontal/ vertical discrimination using the same random array of oriented micropatterns. We specifically avoided scaling our stimuli with eccentricity because we wanted to investigate performance at a given spatial scale and eccentricity (though this is not important because this task exhibits scale invariance over the relevant eccentricity range investigated here; Hess & Dakin, 1997). The resolution of the latter was improved upon by constraining the central element of the path to fall within a defined central zone which was set to a radius of 30 pixels. The exposure duration of 2 s ensured that there was plenty of time for peripheral processing (although pilot results had shown that there was only a very slight improvement in performance between exposure durations of 50 ms and 2 s for both fovea and periphery).

3. Results

In pilot experiments we set out to ensure that peripheral performance in our contour integration task (detection of path embedded in background noise; see Section 2) was not disadvantaged by our initial choice of stimulus parameters. We used Gabor stimuli whose carrier spatial frequency was within the spatial sampling limit of the eccentric loci tested. The contrast of the micropatterns was set to 90% so that they would be of comparable visibility for the fovea and periphery (Lillywhite, Hess & Parker, 1982). Our pilot results showed that the periphery was not selectively disadvantaged by the fixed contrast of our stimuli within the 20–90% contrast range, and that the choice of presentation time was not critical for the foveal/peripheral comparisons. Finally our pilot results indicated that while the periphery is selectively disadvantaged for paths containing small numbers of elements, this was not so for the path length used here (eight elements). The middle element of the path was constrained to go through a central circular region whose radius was 30 pixels which helped localize the eccentricity of our path stimuli.

Fig. 3 displays results for two observers in which we compare the performance of their fovea (unfilled symbols) and two eccentric retinal loci (filled symbols) as a function of path angle. Each datum is the result of 100 forced choice trials. In all cases performance was reduced in the periphery, especially for curved paths.

In a subsequent series of experiments we sought the reason for this reduced performance. Our pilot results had shown that this was unlikely to be due to contrast, presentation duration or path length. Another possibility is that the normal periphery may have defective orientation discrimination and that, since orientation is the key linking feature for these paths, performance is consequently reduced. To assess the possible influence of this factor we introduced orientation noise into the stimuli by allowing the element orientation about the prescribed path to vary according to a Gaussian distribution (Fig. 2). We reasoned along the lines proposed by Pelli (1980) for luminance noise, that if this is a satisfactory explanation then there should be a raised level of intrinsic orientational noise in the periphery for path detection. By varying the amount of stimulus orientational noise, peripheral performance should be further reduced when the stimulus orientational noise far exceeds the elevated intrinsic noise. Thereafter foveal and peripheral performance should be equal as stimulus orientational noise increases. In Fig. 4, results are shown for path detection, at two representative path angles and at two eccentric loci, for two observers as a function of the sigma of the Gaussian distribution which independently controlled the orientation of each element about the prescribed path. As other studies have established (Field, Hayes & Hess, 1993; Hess & Field, 1995) jittering the element angle has a profound effect on path detection. However this effect is, to a first approximation, similar for the fovea and periphery. There is no evidence from these results that the defective performance of the periphery (Fig. 3) is a consequence of a raised level of intrinsic orientational noise. There is no plateau in performance for the periphery at low levels of stimulus orientational noise and performance is not normal in the periphery at high levels of stimulus orientational noise.

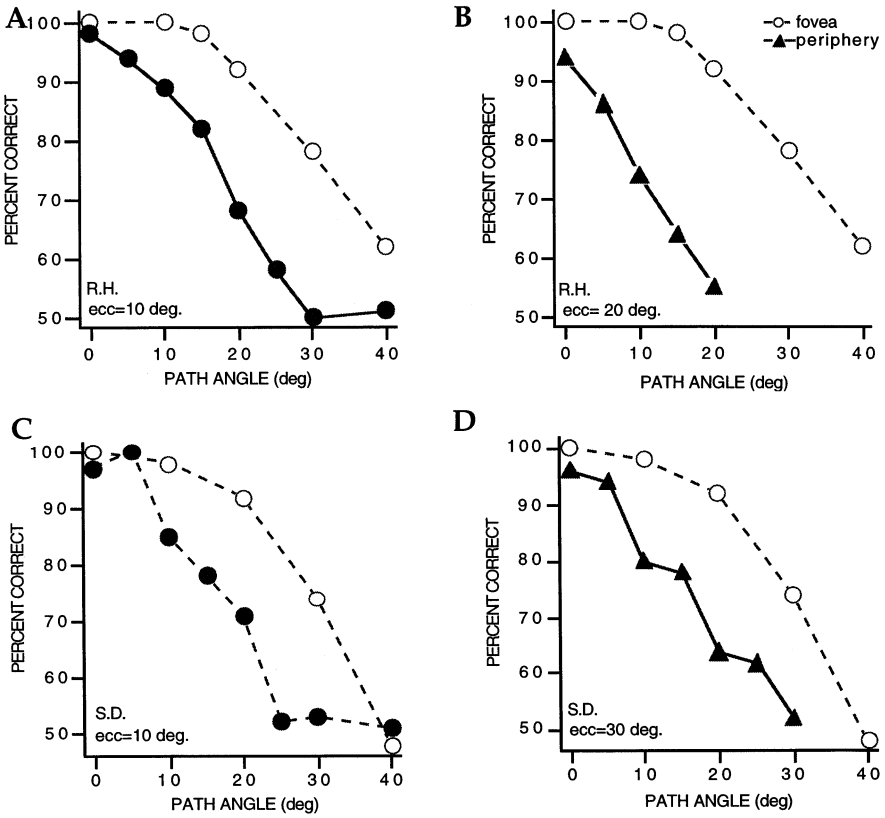

Fig. 3. Path detection is plotted as a function of path angle for the fovea (unfilled circles) and peripheral field (filled circles) for two normal observers.

Another likely explanation for the reduced peripheral performance for contour integration is the raised level of positional uncertainty that is a characteristic of the periphery both at (Levi, Klein & Aitsebaomo, 1985) and below (Hess & Hayes, 1994) the acuity limit. Linking the path elements to form a perceptual contour depends on both orientation and distance and can be expressed in terms of a neural 'association field' (Field, Hayes & Hess, 1993). Positional uncertainty must reduce performance if it is large compared to the dimensions of an 'association field'. To determine whether this may form the basis of a viable explanation for the reduced performance for path detection (Fig. 3) we introduced positional noise into our stimuli by independently varying the 2-D position of the elements comprising the path. This was done by varying the sigma of a Gaussian distribution describing each elements' positional uncertainty about the prescribed path. Results are shown in Fig. 5 for path detection for our observers in which the positional noise of the path stimuli is varied for representative path angles. Unlike the case for orientational noise, these results suggest that the reduced performance seen in Fig. 3 is due to a raised level of intrinsic positional noise in the periphery. The performance of the periphery is less affected by low levels of stimulus positional noise and is similar to normal at high levels of stimulus positional noise. The level of raised intrinsic positional uncertainty can be approximated by the level of stimulus uncertainty necessary to bring the performance of the fovea and periphery together.

It would seem on the basis of the above results that a raised level of positional uncertainty within the periphery could account for some or all of the reduced performance when the stimulus elements were perfectly positioned along the prescribed path. If it totally accounts for the decrement in performance then we can conclude that contour integration per se necessary to solve this task is normal in the periphery. If it only accounts for a part of the performance decrement then a deficit more central to the disarray may be implicated. For this reason we set out to measure the intrinsic positional uncertainty associated with this task at each eccentric locus and to assess whether it represents the complete explanation for the reduced performance in this task (Fig. 3).

To estimate the level of intrinsic positional uncertainty for this task we first measured the incremental threshold of the periphery for positional sensitivity using paths devoid from their background elements. Two presentations were given, one in which the elements were perfectly aligned along a path and another in which each elements' 2-D position about an identical path was varied according to a Gaussian random vari-

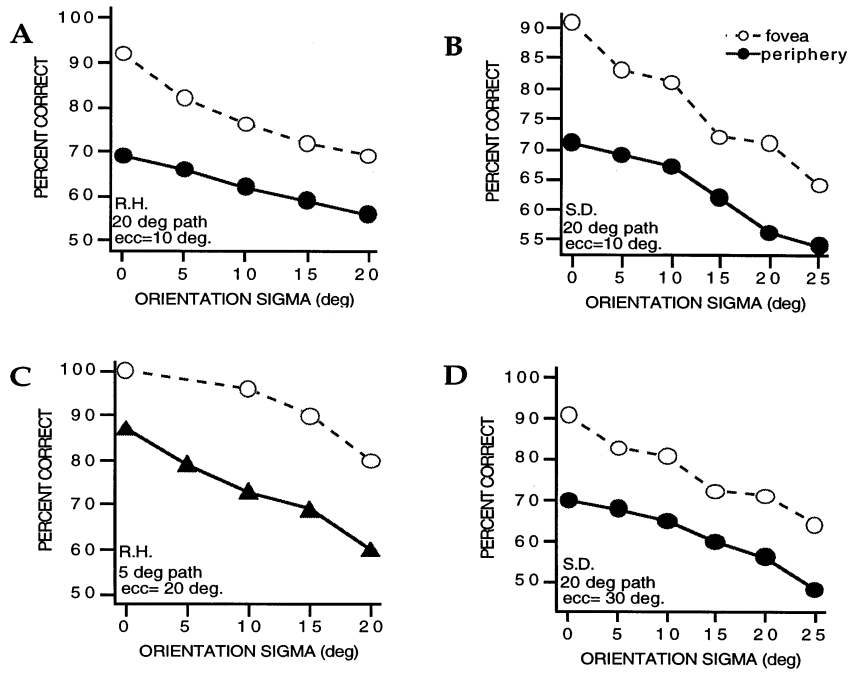

Fig. 4. Comparison of path detection for the fovea (unfilled symbols) and periphery (filled symbols) of two normal observers as a function of the extent (sigma of the Gaussian distribution) to which the orientation of individual path elements is randomized. Each subject was tested at two representative path angles and eccentric loci.

able. A staircase procedure was used to collect psychometric data and a threshold was derived by fitting a Weibull function (see Section 2). This was done for a number of different path angles for each eccentric locus. This gives the incremental positional uncertainty of the eccentric locus corresponding to some unknown intrinsic pedestal within the periphery which we wanted to derive. To estimate this intrinsic pedestal of uncertainty we repeated these measurements on the fovea but this time the incremental threshold was fixed at that previously found for the eccentric locus and the pedestal was varied. This allowed us to estimate what pedestal corresponded to the incremental sensitivity of the eccentric locus. We took this as our estimate of the intrinsic pedestal of uncertainty in the eccentric locus for that particular path angle. This procedure was repeated for a range of different path angles for each subject and a number of eccentric loci. These results are shown in Fig. 6. In this graph, the incremental threshold for the positional uncertainty of the eccentric locus is plotted against the subsequently measured pedestal positional uncertainty measured for the fovea (unfilled symbols for RH and filled symbols for SD). Results are shown for three different path angles (10, 20 and 30°). The solid lines and crosses represent the increment detection function for this positional uncertainty task for a normal fovea. The results are consistent with the idea that the periphery has a raised level of positional uncertainty which elevates its incremental positional thresholds. Similar estimates of the internal pedestal of positional uncertainty were found at the two eccentric loci (10°-circles; 20° (RH) or 30° (SD)-triangles). These results for a string of elements differ from those previously reported for individual elements. In the latter case, positional accuracy has been shown to increase with eccentricity (e.g. Hess & Hayes, 1994)

Having obtained estimates of the intrinsic positional uncertainty pedestal in the periphery of our subjects we tested whether these levels of uncertainty could account for all of the performance decrement previously measured for path detection (Fig. 3). We did this by comparing the original results for the fovea and periphery of each subject measured with perfectly aligned paths (stimulus positional uncertainty of zero as in Fig. 3) with that measured for the fovea with a stimulus positional uncertainty equal to the intrinsic pedestal of uncertainty previously estimated at each eccentric loci. We reasoned that if the fovea with a stimulus positional uncertainty equal to that of the eccentric locus performed comparably to that of the eccentric locus for perfectly aligned paths (stimuli having zero positional uncertainty) then positional uncertainty is a complete explanation for the performance decrement previously described in Fig. 3. These results are shown in Fig. 7 where the previous results of Fig. 3 are compared with new results for the fovea using a stimulus with a positional uncertainty equal to the intrinsic uncertainty of the periphery (unfilled bow-ties). In all cases an explanation based solely on a raised level of positional uncertainty fails to adequately account for the previously poorer path detection exhibited by the periphery.

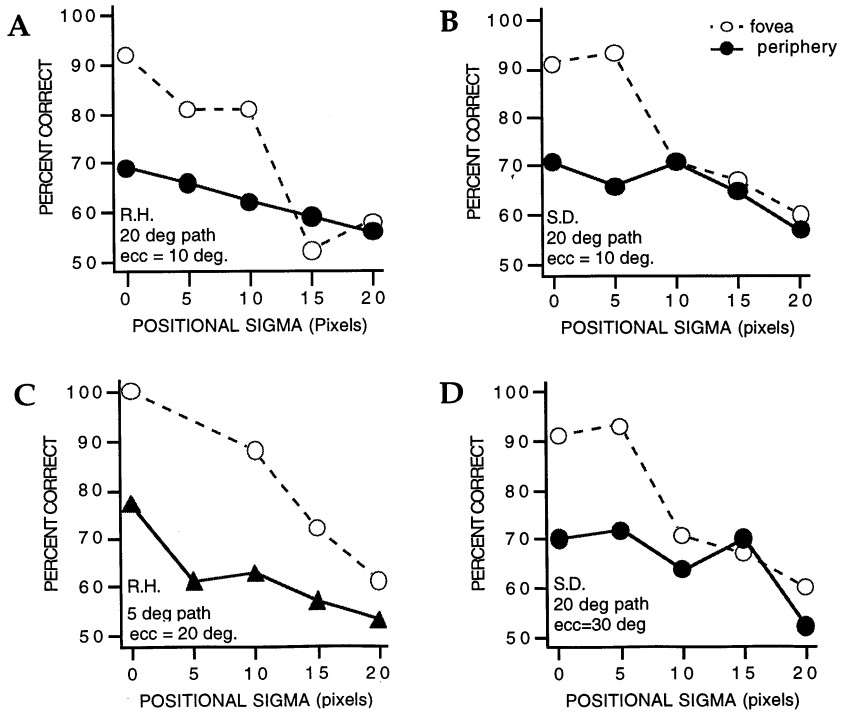

Fig. 5. Comparison of path detection for the fovea (unfilled symbols) and periphery (filled symbols) as a function of the extent (sigma of the Gaussian distribution) to which the 2D positions of individual path elements are randomized. Each subject was tested at two representative path angles and eccentric loci.

One intriguing feature of peripheral performance on this task is that performance is initially reduced at 10° but remains approximately constant at this level out to the furthest eccentricity for which the micropatterns were visible (i.e. 30°). While it has been claimed that simple filtering without orientation linking operations cannot explain foveal contour integration (Field, Hayes & Hess, 1993) this has never been subjected to a quantitative test and such an explanation would provide a simple account for why performance does not deteriorate with eccentricity so long as the micropatterns are still visible. Fig. 8 shows results for two observers for foveal (dashed curve) as well as peripheral (filled symbols) path detection (10–30° eccentricity). Beyond 30° the contrast of the individual micropatterns is below threshold. The solid line represents the prediction based on simple linear filtering without any subsequent orientation linking operations (see Appendix A for details). This provides the floor level of performance above which specialized orientation linking interactions between cells need to be invoked. While such interactions clearly do need to be invoked for the fovea (in line with the predictions of Field, Hayes & Hess, 1993), they are apparently unnecessary to explain the peripheral data. chi-square values for the fit of the model to data are given in Table 1, and do not indicate a significant difference between observed psychophysical performance and predictions. Thus the peripheral data are amenable to an explanation based on filtering at a series of independent orientations devoid of inter-cellular orientation interactions.

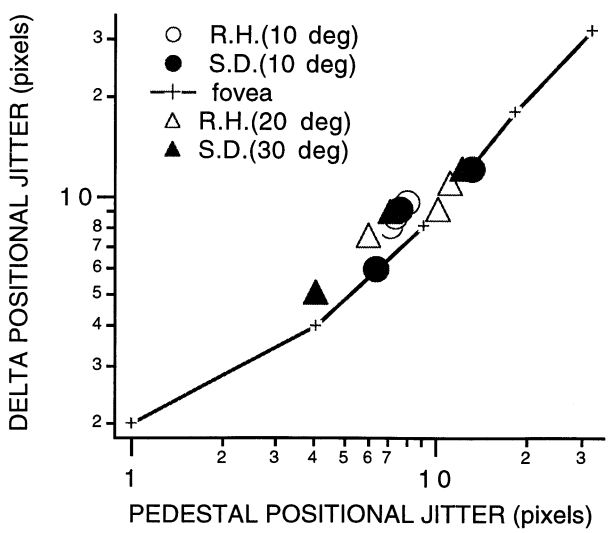

Fig. 6. Comparison of the positional uncertainty thresholds for the periphery plotted against corresponding pedestal positional uncertainty thresholds for the fovea. The solid line and crosses define the increment threshold function for positional accuracy for the fovea.

An obvious test of this conclusion is to construct paths from micropatterns of alternating phase (i.e. alternating by 180°) which would greatly reduce the

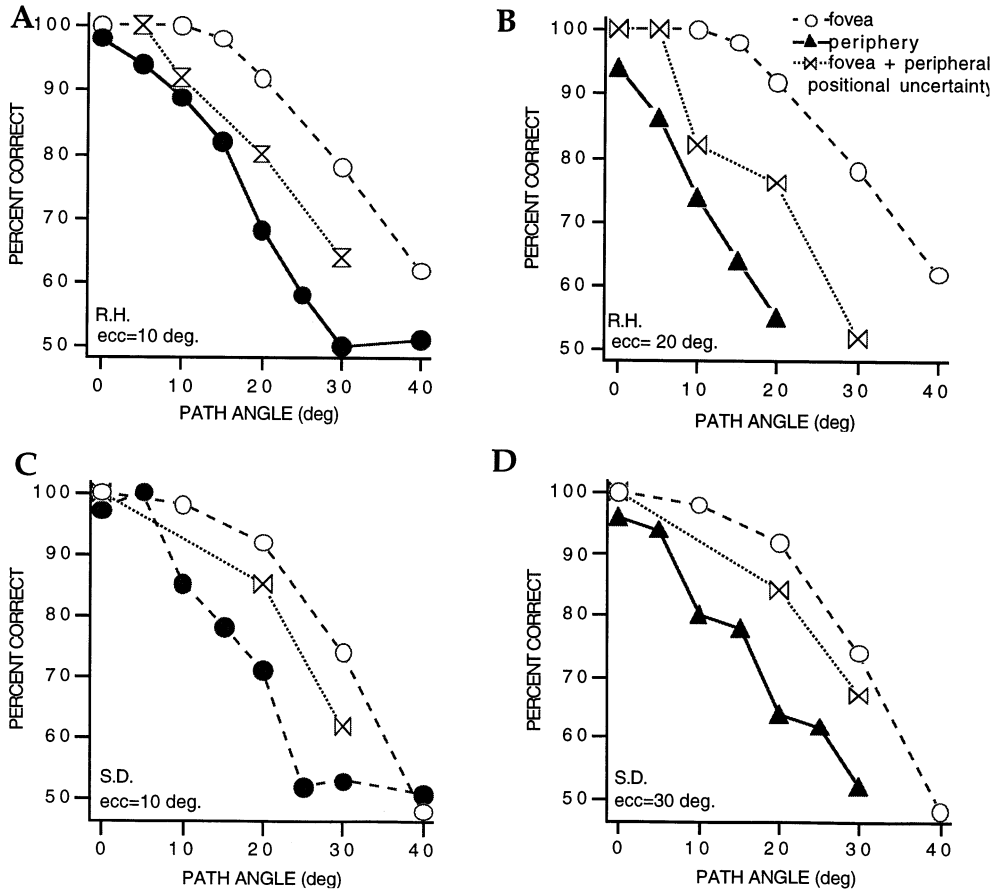

Fig. 7. Path detection is plotted as a function of path angle for the fovea (unfilled circles) and periphery (filled circles) for two observers. The open bow-ties are for the fovea with the intrinsic positional uncertainty pedestal estimated for the eccentric loci.

efficiency of such filtering operations at independent orientations for extracting paths embedded in a field of background elements. Field, Hayes & Hess (1997) have previously shown that foveal performance is only slightly reduced for stimuli alternating in phase by 90 or 180°. This is further support for the need to invoke specialized inter-cellular linking operations for foveal viewing since simple filtering would not be expected to support performance for such stimuli. Fig. 9 shows a comparison between foveal (A and B) and peripheral viewing (C and D to 10° eccentricity; E and F to 20° eccentricity) for paths of the same phase (unfilled symbols-dashed line) compared with ones which alternate in phase by 180° (filled symbols-dashed line). Performance is only slightly reduced with phase-alternating paths in the fovea and at 10° eccentricity, and is far above that predicted by simple filtering for such a stimulus (solid line). However beyond 10° performance for these stimuli, no matter what the path angle, is reduced to chance levels as would be predicted by simple filtering without any inter-cellular linking operations. Similar results (not displayed) were found at 25 and 30° eccentricities.

4. Discussion

Peripheral visual function differs from its foveal counterpart in a number of important respects, most of which are thought to have a postreceptoral basis. These include threshold contrast sensitivity (Robson & Graham, 1981; Pointer & Hess, 1989) and positional uncertainty (Westheimer, 1982; Levi, Klein & Aitsebaomo, 1985; Hess & Hayes, 1994). Neither of these known factors can account for the reduced performance of the periphery on our contour integration task. The individual micropatterns were well within the spatial sampling limitations of the periphery (Wang, Thibos & Bradley, 1996), micropatterns of suprathreshold contrast were used in a task which does not display a contrast dependence above 10–20% contrast, and the intrinsic positional uncertainty of each eccentric locus tested was estimated and controlled for. The periphery appears to be selectively defective at integrating curved contours. This is not a consequence of broader orientation bandwidths of peripheral detectors because there is no evidence of a raised level of intrinsic orientational noise in the periphery. We conclude that the rules by which

cellular outputs are 'associated' differ in fovea and periphery.

The question is whether this difference is fundamental or not. A subjective difference between doing this task in the fovea and periphery is that in the latter case paths appear as a continuous fused feature, as if blurred along their length. Straight paths appear as blurred luminance defined lines and only locally straight segments are seen in curved paths. This is suggestive of a simple filtering mechanism working at a number of independent orientations being used in the periphery and could account for the finding that peripheral path performance is not only dramatically reduced from that of the fovea but also it does not vary greatly with eccentricity. This explanation gains further support from the fact that a simple filtering prediction is sufficient to account for the reduced performance of the peripheral field. The acid test is whether paths composed of Gabors alternating in contrast polarity can be detected in the periphery. Such paths defy a simple linear filtering prediction and can be easily detected in the fovea. The fact the periphery is 'blind' to such paths beyond 10° again suggests that its original path performance was based on simple linear filtering at fixed orientations devoid of any orientation linking operation.

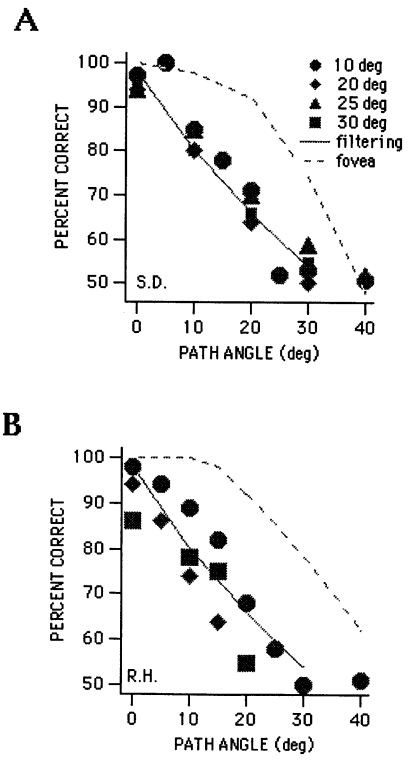

Fig. 8. Path performance for fovea (dashed curve) and for periphery (10–30°-filled symbols). In the periphery but not in the fovea, performance can be predicted on the basis of simple filtering at each of a number of independent orientations without the need to invoke inter-cellular orientation linking operations (see Appendix A for details).

Our conclusion is that beyond about 10° of eccentricity, the visual system relies on simple filtering at independent orientations rather than inter-cellular orientation linking operations to extract contours. This may represent an important economy in the coding of visual information. Linking operations between cells have been considered in two quite different ways in terms of their underlying physiology. Some consider the long range connections between cells with similar orientation preference the physiological basis of linking (T'so & Gilbert, 1988; Gilbert & Wiesel, 1989) Whereas others consider it to be due the synchronized oscillations that have been observed between cells (von der Malsburg, 1983; von der Malsburg & Singer, 1988; Engel, König, Kreiter, Schillen & Singer, 1992; Kreiter & Singer, 1994) What ever the explanation, the present results suggest that there should be fundamental differences between cells located in central and peripheral regions in either their long range connections and/or the degree to which they display synchronized oscillations.

Acknowledgements

This work was supported by a grant (# MT 10818) from the Medical Research Council of Canada. We are very grateful to R. Demanins for her help in all aspects of this project and Cristyn Williams for comments on the manuscript.

Appendix A. Stimulus parameters in screen units

Stimulus parameter	Value
Gabor patch size (pixels)	37
Frequency of Gabor carrier (c/pixels)	0.05
Carrier phase	sine
Space constant of Gaussian (pixels)	8.0
Element contrast (%)	90
Oriented	y
Number of path elements	8
Start index of elements that must be in center	4
End index of elements that must be in center	4
Radius of central region (pixels)	30
Path step size (pixels)	67
Jitter of path angle (°)	4
Standard deviation of element positions (pixels)	0 varied in one experiment
Standard deviation of element orientations (°)	0 varied in one experiment

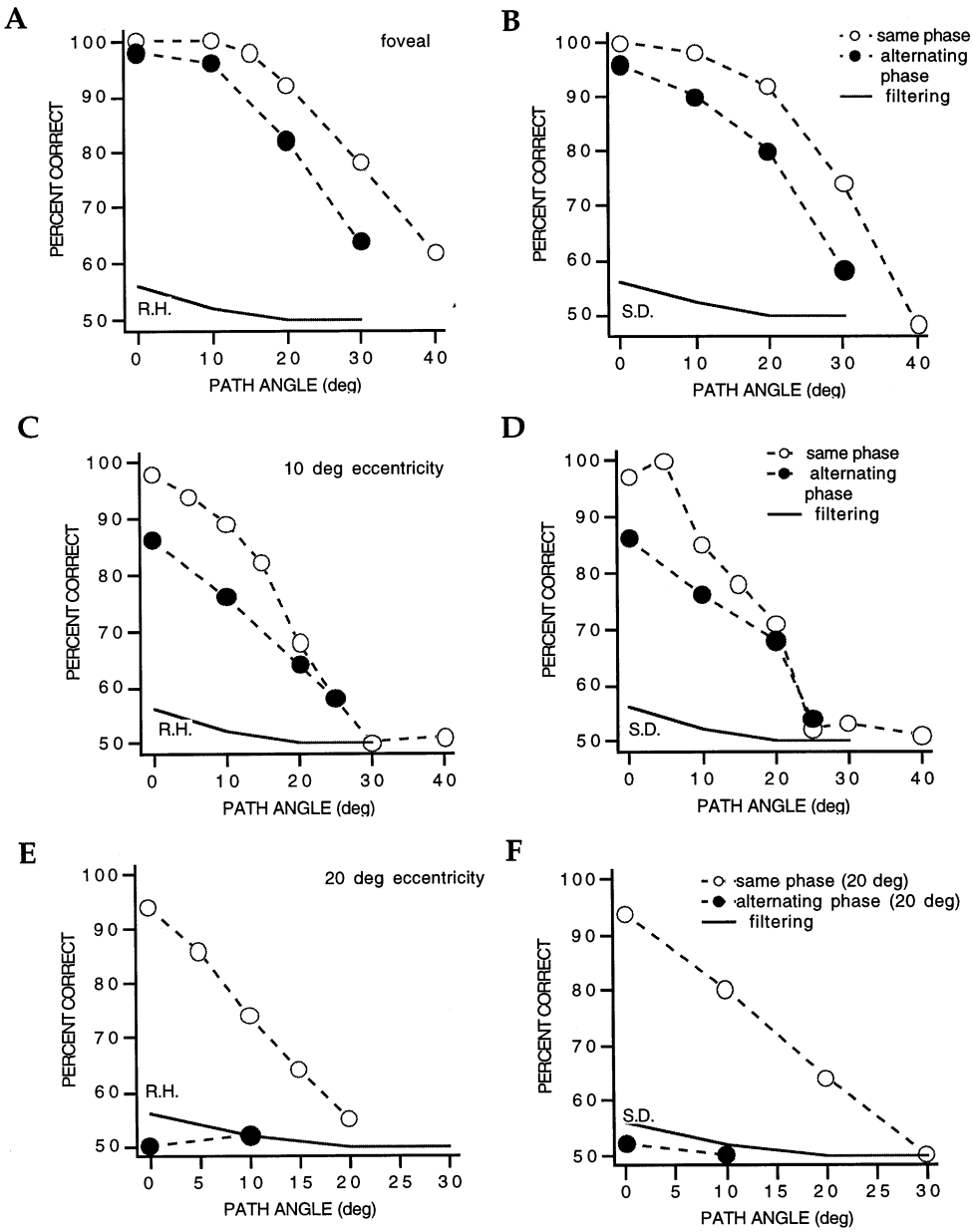

Fig. 9. Foveal (A and B) and peripheral (C–D) path performance compared for paths composed of micropatterns of the same phase (unfilled symbols) and alternating phase (filled symbols). The solid line represents the prediction for simple filtering for paths comprising elements of alternating phase.

Number of cells, x-direction (pixels	13
Number of cells, y-direction (pixels)	13
Cell size (pixels)	48
Duration (ms)	2000

Appendix B. Modeling of path discrimination

B.1. The model

Images are initially convolved (Fig. 10b) with a two-dimensional Difference-of-Gaussian (DoG) filter, composed of a DoG in the y-direction multiplied by a Gaussian in the x-direction: Eq. (3)

$$W(x,y)=\left[\exp(-x_t^2/2\sigma^2)-\frac{1}{2.23}\exp(-x_t^2/2(2.23\sigma)^2)\right]\times\exp(-y^2/2(3\sigma)^2) \quad (3)$$

where refers to the standard deviation of the positive Gaussian function and (x_t, y_t) are coordinates rotated by angle

$$x_t = x\cos\phi + y\sin\phi$$
$$y_t = y\cos\phi - x\sin\phi \quad (4)$$

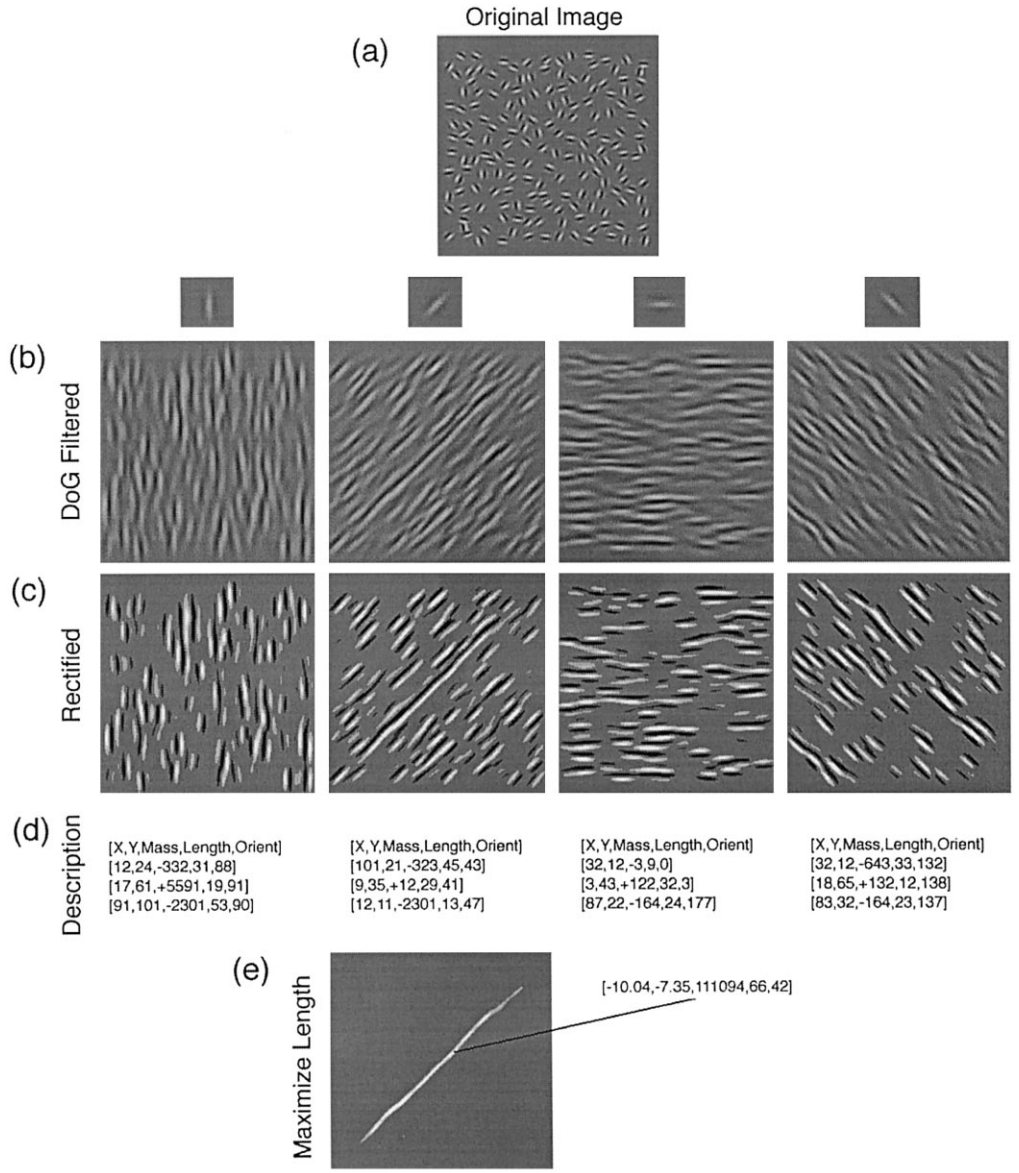

Fig. 10. A model of path detection with no intra-filter interaction. Images are convolved with a bank of oriented filters, rectified, and a description of resulting features constructed at each orientation. The longest feature present, across all orientations, is selected as the path.

Parameters of the DoG are based on those derived by Phillips & Wilson (1983). The exact form of this filter is not critical; any kernel with similar orientation and spatial band-width would suffice. The model used a single filter size of $\sigma = 4.5$ pixels, and orientations of $\phi = 0$–$175°$ in steps of 15°.

The filtered image is next thresholded (Fig. 10c), by removing gray levels which are less than one standard deviation from zero (the mean gray level):

$$R(x, y) = I(x, y) \quad \text{if } |I(x, y)| \text{ gt;} S$$

$$R(x, y) = 0 \quad \text{otherwise} \tag{5}$$

where S is the gray level standard deviation over all pixels. The exact type of non-linearity is not critical; it merely serves as a means of delineating features in the image.

The 'blobs' which result from this operation are converted into a symbolic representation using Watt's image description scheme (Fig. 10d; Watt, 1988, 1991). Specifically a description of blob number i was of the form:

$$(cx_i, cy_i, \mu_i, \lambda_i, \theta_i) \tag{6}$$

where (cx_i, cy_i) is the centroid, μ_i the mass, λ_i the length and θ_i the orientation of the blob. This form of description is reminiscent of Marr's primal sketch (Marr, 1976, 1982).

Finally, given a set of image descriptions across all orientations (at one spatial scale) the path was ex-

tracted by simply identifying the blob with the greatest length (Fig. 10e).

The only free parameters of the model are the threshold and the filter size. Pilot studies indicated that threshold (from 0.5 to 2.0 gray level standard deviations) did not greatly affect predictions. Filter size was set to optimize performance; the predictions from the model could not be improved by varying either of the model's free parameters.

B.2. Simulation methods

B.2.1. Stimuli

Stimuli were generated using exactly the same procedure as described in the psychophysical methods above. However textures (and filters) were down-sampled to 128 pixels square prior to convolution.

B.2.2. Procedure

Fifty images were generated at each of nine path angles, from 0 to 80° in steps of 10°. Each image was then down-sampled and filtered with the filter-bank described above, half-wave rectified and a description calculated. Finally the blob with the greatest length was selected from all descriptions, across all orientations. The length of this blob was recorded for this image. Having made this estimate of the longest feature from each image, an estimate of discriminability from noise was estimated by comparing length estimates for each path angle from estimates derived from a noise image.

References

Anderson, S. J., Mullen, K. T., & Hess, R. F. (1991). Human peripheral spatial resolution for achromatic and chromatic stimuli: limits imposed by optical and retinal factors. *Journal of Physiology* (*London*), *442*, 47–64.

Engel, A. K., König, P., Kreiter, A. K., Schillen, T. B., & Singer, W. (1992). Temporal coding in the visual cortex: new vistas on integration in the nervous system. *Trends in Neurosciences*, *15*, 218–226.

Field, D. J., Hayes, A., & Hess, R. F. (1993). Contour integration by the human visual system: evidence for a local 'association field'. *Vision Research*, *33*, 173–193.

Field, D. J., Hayes, A., & Hess, R. F. (1997). The role of phase and contrast polarity in contour integration. *Investigative Opthalmology and Visual Science*, *38*, 999.

Gilbert, C. D., & Wiesel, T. N. (1989). Columnar specificity of intrinsic horizontal and corticocortical connections in cat visual cortex. *Journal of Neuroscience*, *9*, 2432–2442.

Hess, R. F., & Dakin, S. C. (1997). Absence of contour linking in peripheral vision. *Nature*, *390*, 602–604.

Hess, R. F., & Field, D. J. (1995). Contour integration across depth. *Vision Research*, *35*, 1699–1711.

Hess, R. F., & Hayes, A. (1994). The coding of spatial position by the human visual system: effects of spatial scale and retinal eccentricity. *Vision Research*, *34*, 625–643.

Hess, R. F., & Watt, R. J. (1990). Regional distribution of the mechanisms that underlie spatial localization. *Vision Research*, *30*, 1021–1031.

Kovacs, I., & Julesz, B. (1993). A closed curve is much more than an incomplete one: effect of closure in figure-ground segmentation. *Proceedings of the National Academy of Sciences of the United States of America*, *90*, 7495–7497.

Kreiter, A. K., & Singer, W. (1994). Global stimulus arrangement determines synchronization of neuronal activity in the awake macaque monkey. *European Journal of Neuroscience* (*Supplement*), *7*, 153.

Levi, D. M., Klein, S. A., & Aitsebaomo, A. P. (1985). Vernier acuity, crowding and cortical magnification. *Vision Research*, *25*, 963–977.

Lillywhite, P. G., Hess, R. F., & Parker, A. (1982). How effective is contrast constancy? *Investigative Ophthalmology and Visual Science* (*Supplement*), *22*, 207.

Marr, D. (1976). Early processing of visual information. *Proceedings of the Royal Society of London*, *B*, *275*, 483–534.

Marr, D. (1982). *Vision*. San Francisco: Freeman.

McIlhagga, W. H., & Mullen, K. T. (1996). Contour integration with colour and luminance contrast. *Vision Research*, *36*, 1265–1279.

Pelli, D. G. (1980). The quantum efficiency of vision. In C. Blakemore, *Vision coding and efficiency*. Cambridge: Cambridge University Press.

Phillips, G., & Wilson, H. (1983). Orientation bandwidths of spatial mechanisms measured by masking. *Journal of the Optical Society of America*, *62*, 226–232.

Pointer, J. S., & Hess, R. F. (1989). The contrast sensitivity gradient across the human visual field: emphasis on the low spatial frequency range. *Vision Research*, *29*, 1133–1151.

Robson, J. G., & Graham, N. (1981). Probability summation and regional variation in contrast sensitivity across the visual field. *Vision Research*, *21*, 409–418.

T'so, D. Y., & Gilbert, C. D. (1988). The organization of chromatic and spatial interactions in the primate striate cortex. *Journal of Neuroscience*, *8*, 1712–1727.

von der Malsburg, C. (1983). How are nervous systems organized? In E. Basar, H. Flohr, H. Haken, & A. J. Mandell, *Synergetics of the brain*. Berlin: Springer Verlag, 238–249.

von der Malsburg, C., & Singer, W. (1988). Principles of cortical network organisation. In P. Rakic, & W. Singer, *Neurobiology of neocortex*. Chichester: Wiley, 69–99.

Wang, Y., Thibos, L. N., & Bradley, A. (1996). Undersampling produces non-veridical motion perception, but not necessarily motion reversal, in peripheral vision. *Vision Research*, *36*, 1737–1744.

Watt, R. J. (1988). *Visual processing*: *computational*, *psychophysical and cognitive research*. London: Lawrence Erlbaum.

Watt, R. J. (1991). *Understanding vision*. London: Academic Press.

Wertheim, T. (1994). Uber die indirekte ßchocharfe. *Zeitschrift Psychologie*, *7*, 172–189.

Westheimer, G. (1982). The spatial grain of the perifoveal visual field. *Vision Research*, *22*, 157–162.